

Multifractal detrended fluctuation analysis of ionospheric total electron content data during solar minimum and maximum



E. Chandrasekhar^{a,*}, Sanjana S. Prabhudesai^b, Gopi K. Seemala^c, Nayana Shenvi^b

^a Department of Earth Sciences, Indian Institute of Technology Bombay, Powai, Mumbai 400076, India

^b Department of Electronics & Telecommunication Engineering, Goa College of Engineering, Goa 403401, India

^c Indian Institute of Geomagnetism, New Panvel, Navi Mumbai 418023, India

ARTICLE INFO

Keywords:

Ionospheric TEC

Multifractal detrended fluctuation analysis

Lunar tidal effects

ABSTRACT

The spatio-temporal variations in ionospheric vertical total electron content (TEC) data, which often reflect their scale invariant properties, can well be studied with multifractal analysis. We discuss the multifractal behaviour of TEC recorded at a total of 27 stations confined to a narrow longitude band (35°W–80°W) spanning from equator to high-latitude regions (30°S to 80°N) (geographic coordinates) during solar minimum (2008) and solar maximum (2014), using multifractal detrended fluctuation analysis (MFDFA). MFDFA provides an understanding of the multifractal scaling behaviour of a signal using the multifractal singularity spectra and the generalised Hurst exponents as diagnostic tools. The objectives of this study are to (i) understand the latitudinal dependence of the multifractal behaviour of TEC, (ii) compare the multifractal behaviour of TEC corresponding to the well-known 27-day variation (solar rotation period) and its harmonics and the 1-day (solar diurnal) periodicities, during 2008 and 2014 and (iii) understand the lunar tidal influence on TEC. Results indicate that except for the 1-day period, the TEC at all other periods shows a higher degree of multifractality during solar maximum compared to solar minimum. Further, irrespective of the solar activity, the degree of multifractality in general decreases with increase in period for all latitude zones for periods of 27-day and its harmonics. However, the 1-day period exhibits monofractal behaviour regardless of the solar activity. The influence of semi-lunar tidal effects (having a periodicity of about 14.5 days) as a function of latitude is clearly seen in the 13.5-day periodicity (i.e., the 2nd harmonic of 27-day variation) of TEC. It manifests in the form of decreasing differences in the widths of the multifractal singularity spectra corresponding to the years 2008 and 2014, with increase in latitude. Results are discussed in the light of these observations.

1. Introduction

Investigations of ionospheric total electron content (TEC) have been the topic of acute research interest for over several decades. As the demand for trans-ionospheric communication and navigation systems is increasing in the applications such as navigation of vehicles, aircrafts and even satellites, the measurements as well as characterization of ionospheric TEC has become important for making appropriate range delay corrections. Also, TEC is an important parameter in ionospheric studies, which quantifies the short and long term changes of upper atmosphere during major phenomena caused by solar activity, meteorological influences, etc. Ionospheric TEC exhibits a large dependence on the seasonal and solar activity and show large-scale regional differences across different regions on the globe. Such a naturally produced complex spatio-temporal behaviour of TEC exhibits truly non-stationary and non-linear phenomena of the ionosphere. Therefore, suitable mathematical

techniques need to be employed for characterizing and better understanding of its spatio-temporal behaviour. However, most literature on the TEC studies carried out either by using GPS measurements or by using radio-beacon measurements provides a graphical and visual description of the behaviour of TEC, be it on its spatio-temporal behaviour or its comparative behaviour during solar quiet and disturbed days, or on its seasonal dependency. Applications of latest signal analysis techniques, such as wavelet transformation, fractal and multifractal analyses and empirical mode decomposition technique, for better interpretation of this important ionospheric behaviour have been only a few. Therefore it becomes important and necessary to apply such novel signal analysis techniques to the available relevant data sets and help improve the understanding of the dynamics of the ionosphere at local and regional scales with apt interpretation.

Several investigations have been undertaken to study the ionospheric TEC data using global and/or regional GPS network (Pröls,

* Corresponding author.

E-mail address: esekhar@iitb.ac.in (E. Chandrasekhar).

1993; Otsuka et al., 2002; Meza et al., 2005; Rama Rao et al., 2006; Huang, 2008; Fernandez et al., 2012 and references therein). Using the Indian GPS network data, Dasgupta et al. (2007) studied effect of TEC on space navigation, particularly when TEC is high in equatorial regions. A variety of comparative studies on ionospheric TEC derived for Indian region with those of International Reference Ionosphere (IRI) are available (Bhuyan and Borah (2007) and references therein). Gulyaeva (1999) used statistical methods for TEC modelling (see Liu and Chen (2009) and references therein). Wavelet analysis and spectral methods were employed (i) to characterize tidal amplitude fluctuations in the lower thermosphere (Pancheva and Mukhtarov, 2000) and to characterize TEC at regional scales (Grinsted et al., 2004; Krankowski et al., 2005; Fagundes et al., 2005; Pancheva et al., 2006 (and references therein); Borries et al., 2007; Wang et al., 2008), (ii) to study ionospheric irregularities from TEC data (Pervak et al., 2008) and (iii) to determine the ionospheric response during a magnetic storm using the vertical TEC data (Fernandez et al., 2012). Lin (2010, 2011a,b) applied principal component analysis technique to understand the TEC behaviour before and after the occurrence of earthquakes. Empirical orthogonal function (EoF) analysis was employed for global TEC modelling (Ercha et al., 2012) and for characterizing spatio-temporal behaviour of TEC at regional scales (Shagimuratov et al., 2013; Zheng et al., 2016).

As well known, the ionospheric TEC has been proved to display not only large-scale spatio-temporal behaviour, but also a clear dependence on solar activity (Klobuchar, 1991) and thus the TEC concentrations in the F-region of ionosphere are higher during geomagnetically disturbed periods than during quiet periods. However, notwithstanding to such previous observational evidences, we quantify and discuss the degree of stochasticity in the ionospheric TEC corresponding to the solar minimum (2008) and solar maximum (2014) years, using a nonlinear data analysis technique called, multifractal detrended fluctuation analysis (MFDFA) in the present study. The MFDFA, which in fact, is a generalization of detrended fluctuation analysis (DFA), provides a comprehensive understanding of the multifractal behaviour of the signals through the multifractal singularity spectrum as well as the Hurst exponents (see Kantelhardt et al. (2002), Subhakar and Chandrasekhar (2016) for details). The main objectives of this study are to (i) understand the latitudinal dependence of the multifractal behaviour of TEC, (ii) compare the multifractal behaviour of TEC corresponding to the well-known 27-day variation (solar rotation period) and its harmonics and the 1-day (solar diurnal) periodicities, during 2008 and 2014 and (iii) understand the lunar tidal influence on TEC (see Siddiqui et al. (2015)). The organization of the chapter is as follows. Section 2 describes the data selection and processing. Section 3 provides a detailed description of the MFDFA technique. Section 4 discusses the obtained results and Section 5 contains the conclusions of the study.

2. Data base

GPS data for the present study has been obtained from Scripps Orbit and Permanent Array Centre (SOPAC), California (<http://sopac.ucsd.edu/dataBrowser.shtml>), which maintains a repository of GPS data from various IGS (International GNSS Service) stations (<http://igs.org/network>). Data from a total of 27 stations, confined to a narrow longitude band (35–80°W) spanning from equator to high-latitude regions (30°S to 80°N) (geographic coordinates) corresponding to solar minimum (2008) and solar maximum (2014) years were procured. Fig. 1 depicts the map showing the geographical location of several stations, whose data were used in the present study. These stations were selected based on the maximum availability of data with least number of missing points for the chosen two years. The data obtained were in GPS RINEX (Receiver Independent Exchange) format, which were converted into mean (two-sigma iterated) vertical total electron content (TEC) sampled at 1-min interval. This was done using the

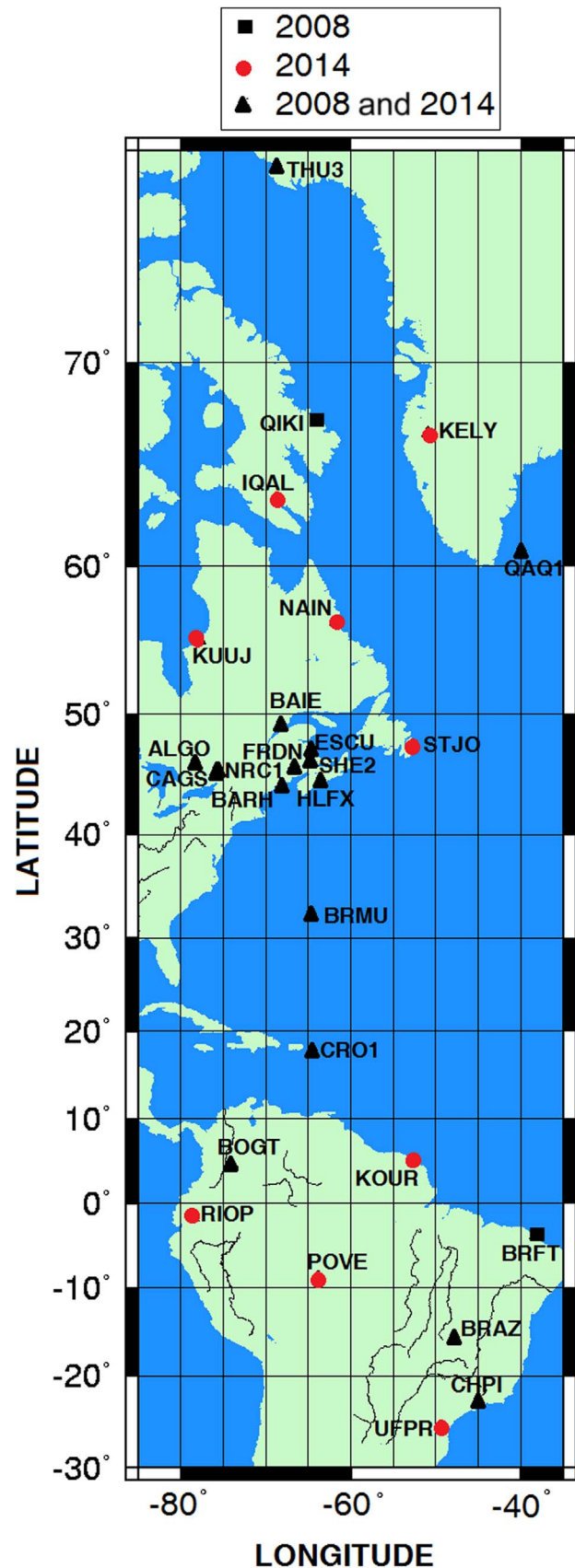


Fig. 1. Geographical location of the IGS stations, whose GPS data were used to derive TEC for the present study. The sites are confined to a narrow longitude band extending from equatorial to high latitude regions. TEC data corresponding to the solar minimum (2008) and solar maximum (2014) years of these sites were considered for the present study. Map was generated using GMT of Wessel et al. (2013).

software “RINEX GPS_TEC program” (see Rama Rao et al., 2006; Seemala and Valladares, 2011). In this program, the GPS observables at two frequencies L1 (1575.42 MHz) and L2 (1227.60 MHz) are used to calculate TEC. The ionosphere is a dispersive medium at radio frequencies and affects the GPS signals passing from satellite to ground in different ways. Thus the GPS signals traversing the ionosphere undergoes additional delay proportional to total number of electrons in a cross-sectional volume measured in TEC units. Considering the advantage of the dispersive nature of the ionosphere, the dual frequency GPS receivers can be used to measure the ionospheric delay. The ionospheric time delay (t_1 and t_2) at the L1 (of f_1) and L2 (of f_2) carrier frequencies is given by (Klobuchar, 1996)

$$t_1 = 40.3 \left(\frac{TEC}{cf_1^2} \right) ; \quad t_2 = 40.3 \left(\frac{TEC}{cf_2^2} \right) \quad (1)$$

where ‘c’ is the speed of light in free space. The difference in delay time between the two frequencies, Δt ($= t_2 - t_1$), is given by

$$\Delta t = \left(\frac{40.3}{c} \right) \times TEC \times \left(\frac{1}{f_2^2} - \frac{1}{f_1^2} \right) \quad (2)$$

Thus, the delay time measured between the L1 and L2 frequencies is used to calculate the TEC along the ray path. The calculation of TEC by the above method using pseudorange data alone produces noise, while the differential carrier phase gives a precise measure of relative TEC variations because the actual number of cycles of phase is not known. Absolute TEC cannot be obtained unless pseudorange is also used. Therefore, use of the pseudorange gives the absolute scale for TEC while differential phase increases measurement accuracy. The estimated TEC is the sum of the slant TEC (STEC), the GPS satellite differential delay, b_s (satellite bias) and the receiver differential delay, b_R (receiver bias), i.e., $TEC = STEC + b_R + b_s$. Therefore, the vertical TEC can be expressed as

$$VTEC = \frac{TEC - (b_R + b_s)}{S(E)} \quad (3)$$

where E is the elevation angle of the satellite in degrees, $S(E)$ is the obliquity factor (or the mapping function) with zenith angle z at the Ionospheric Pierce Point (IPP), defined as (Mannucci et al., 1993; Fedrizzi et al., 2002)

$$S(E) = \frac{1}{\cos(z)} = \left\{ 1 - \left(\frac{R_E \times \cos(E)}{R_E + h_s} \right)^2 \right\}^{-0.5} \quad (4)$$

where R_E is the mean radius of the Earth in km, h_s is the effective height of the ionosphere. VTEC denotes the vertical TEC at the IPP. VTEC estimated using Eq. (3) is used for analysis in the present study. However, it is simply referred to as TEC for convenience. Eq. (3) explains that the TEC is obtained by using the differential satellite biases, which are routinely published by the University of Bern and the receiver bias, which is calculated by minimizing the TEC variability between 0200 and 0600 LT (Rama Rao et al., 2006; Seemala and Valladares, 2011).

The “RINEX GPS_TEC program” facilitates to process the GPS data in batch-processing mode also. This is advantageous particularly while handling larger data sets for TEC data analysis. For more details of this freely-downloadable software (together with user manual), the reader is referred to <http://seemala.blogspot.in/>. The RINEX GPS_TEC software converts each day’s GPS data into its respective TEC data at 1-min. sampling interval. The thus obtained TEC data of each day of the respective years are next concatenated to obtain the yearly TEC data corresponding to each year for each of the 27 stations shown in Fig. 1. Fig. 2 shows such concatenated data of some representative stations of equatorial, mid latitude and high latitude zones corresponding to the years 2008 (Fig. 2a-c) and 2014 (Fig. 2d-f). Table 1 lists the geographic and geomagnetic coordinates of all the stations shown in Fig. 1. For the latitude-wise classification of stations, geomagnetic coordinates were used (Table 2).

2.1. Data processing (interpolation)

MFDFFA technique requires that the data under investigation must be continuous. Therefore, the obtained yearly TEC time series data corresponding to each station was first examined for continuity before proceeding for further analysis. Largely, the data quality at each station was found to be good and there were only a few stations that had missing data for a few days in each year (thanks to the staff of SOPAC for maintaining such high quality data). In the yearly TEC time series, the missing data were accounted for by employing a special linear interpolation procedure that resulted least error. This procedure is described as follows. Generally, the conventional linear interpolation technique works well, when the number of missing data is small

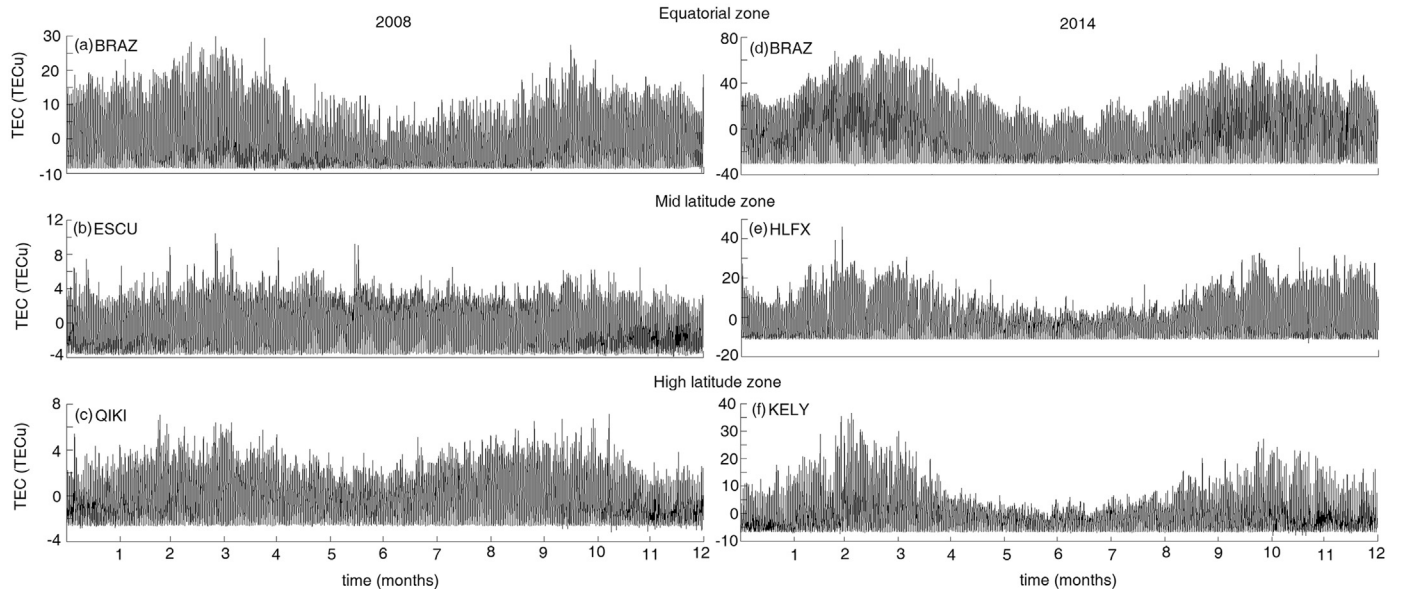


Fig. 2. Concatenated TEC data of representative stations for each of the latitude zones corresponding to solar minimum (a-c) and solar maximum (d-f).

Table 1
Geographic and geomagnetic coordinates of IGS stations used in the present study. The latitude-wise grouping of stations was done based on geomagnetic coordinate system.

Sl. no.	IGS station Code	coordinates (in degrees)			
		Geographic		Geomagnetic	
		Lat.	Long.	Lat.	Long.
1	THU3	76.53	-68.82	86.12	12.99
2	QIKI	67.55	-64.03	76.98	14.61
3	KELY	66.98	-50.94	75.48	35.27
4	IQAL	63.75	-68.51	73.13	6.25
5	QAQ1	60.71	-46.04	68.86	37.47
6	NAIN	56.53	-61.68	65.86	14.79
7	KUUJ	55.27	-77.74	64.72	-6.85
8	BAIE	49.18	-68.26	58.69	5.42
9	STJO	47.59	-52.67	56.43	24.59
10	ESCU	47.07	-64.79	56.52	9.62
11	SHE2	46.22	-64.55	55.66	9.85
12	ALGO	45.95	-78.07	55.45	-6.80
13	FRDN	45.93	-66.65	55.42	7.25
14	CAGS	45.58	-75.8	55.12	-4.00
15	NRC1	45.45	-75.62	54.99	-3.78
16	HLFX	44.68	-63.61	54.09	10.88
17	BARH	44.39	-68.22	53.91	5.26
18	BRMU	32.37	-64.69	41.48	8.92
19	CRO1	17.75	-64.58	27.29	8.54
20	KOUR	5.25	-52.8	14.38	20.32
21	BOGT	4.64	-74.08	14.35	-1.58
22	RIOP	-1.65	-78.65	8.05	-6.17
23	BRFT	-3.87	-38.42	4.32	34.14
24	POVE	-8.70	-63.89	1.00	8.55
25	BRAZ	-15.94	-47.87	-6.95	23.86
26	CHPI	-22.68	-44.98	-13.84	26.11
27	UFPR	-25.44	-49.23	-16.29	21.88

relative to the length of the data. However, in the present case, since there are about 525,600 data points in each year (1440×365) (slightly more in case of 2008, which is a leap year), such a general linear interpolation will not work effectively, even if the data were missing for one day. Therefore, in the present context, the TEC data corresponding to a particular minute of each day is chosen in the entire year-length data sequence. This way, we need to deal with only 365 (or 366) data points at a time for linear interpolation of the missing data within this segment. Once the interpolation corresponding to that particular minute is completed, then the next minute data corresponding to each day in the entire year is considered and linear interpolation is done. This procedure is repeated till all the missing data are interpolated in the entire year-length data sequence corresponding to each station. To test the correctness of this procedure, we have intentionally removed some portions of the data of one of the stations and applied the above procedure to interpolate the removed portion of the data. We then compared the original and interpolated data sets. Fig. 3 depicts such a comparison of the original data (shown in blue) and the interpolated data (shown in red). As seen in Fig. 3, there is a very good agreement between the original data and the interpolated data. The estimated

Table 2
Latitude-wise distribution of IGS stations corresponding to solar quiet year (2008) and active year (2014).

Geomagnetic latitude zone	IGS Stations used	
	2008	2014
High latitude zone (60°N and above)	THU3, QIKI, QAQ1	THU3, KELY, IQAL, QAQ1, NAIN, KUUJ
Mid latitude zone (between 20°N and 60°N)	BAIE, ESCU, SHE2, ALGO, FRDN, CAGS, NRC1, HLFX, BARH, BRMU, CRO1	BAIE, STJO, ESCU, SHE2, ALGO, FRDN, CAGS, NRC1, HLFX, BARH, BRMU, CRO1
Equatorial latitude zone (between 20°S and 20°N)	BOGT, BRFT, BRAZ, CHPI	KOUR, BOGT, RIOP, POVE, BRAZ, CHPI, UFPR

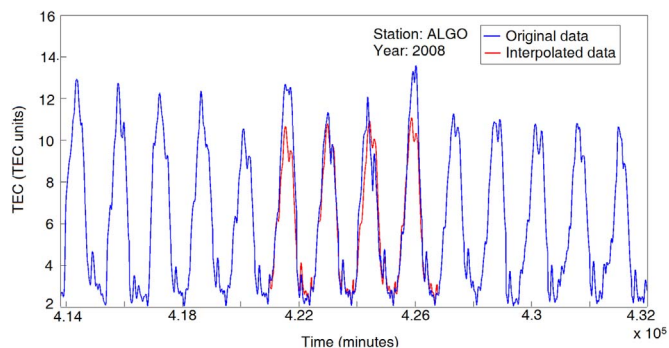


Fig. 3. Comparison of the original (blue) and interpolated (red) TEC data obtained using the new linear interpolation algorithm implemented in the present study. The RMS error between the original and interpolated data is 1.12. (For interpretation of the references to color in this figure legend, the reader is referred to the web version of this article.)

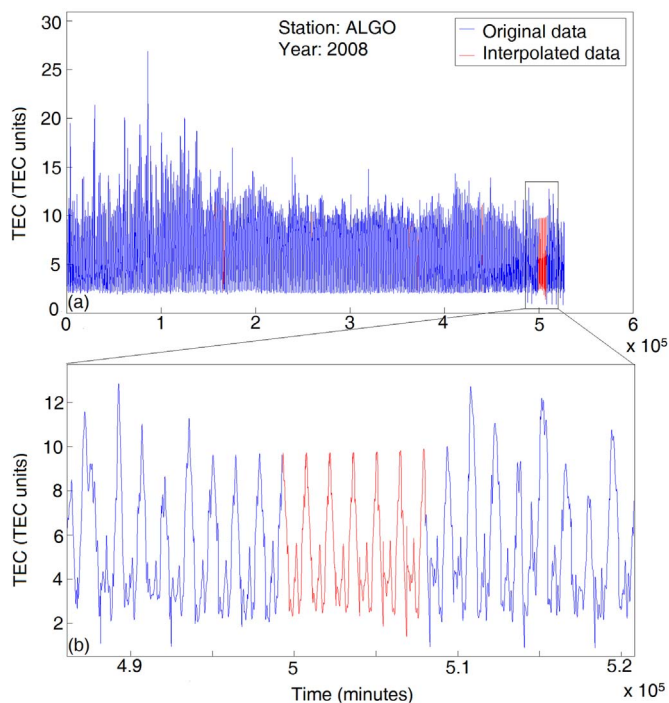


Fig. 4. (a) Original (blue) and interpolated (red) data of one of the stations, ALGO corresponding to the year 2008. Inset (b) depicts the enlarged portion of the interpolated data obtained using the new linear interpolation algorithm implemented in the present study (see Section 2.1) (For interpretation of the references to color in this figure legend, the reader is referred to the web version of this article.)

RMS error between the original and interpolated data is 1.12. Fig. 4 shows the data interpolated by the above method corresponding to one of the stations, ALGO. Fig. 4a shows the raw TEC data in blue and interpolated data in red at missing positions. Fig. 4b shows the expanded version of the interpolated data.

2.2. Data processing (filtering)

Fig. 5 shows the spectrum of the TEC data of one of the mid latitude stations, ALGO, clearly depicting the presence of the well-known periods of solar origin, namely, the 27-day variation and its harmonics (13.5-day and 9-day periods) and the solar diurnal period (1-day). Since the fundamental period of TEC is one day, the dominant presence of 1-day periodicity is clearly seen in the data. However, the frequency resolution of 27-day and its harmonics is rather poor (see the inset in Fig. 5a). This is mainly due to the length of the data (one year only) used in the present study, as the number of cycles of these long periods compared to one-day period, in a one-year data set will be only a few. The TEC time-series data were next subjected to filtering to select only those data corresponding to the above periods to study the spatio-temporal behaviour of TEC for better characterization, as mentioned above. We have applied type-I Chebyshev bandpass filter for filtering the selected periods in the data. The advantage of this filter is that unlike in type-II Chebyshev filter, which has ripples in the stop band, the type-I filter has ripples in the pass band. Additionally, compared to Butterworth bandpass filter, the type-I Chebyshev bandpass filter offers smaller transition bandwidth and steeper roll off, which make the filter more effective for the type of investigations carried out in the present study (see Chapter 8 of Proakis and Manolakis (1996) for more details on different responses of these filters). In fact, on these points, we have tested the responses of both type-I Chebyshev and Butterworth bandpass filters on TEC data and found the former to be more preferable than the latter concerning the selection of as narrow band of frequencies as possible centered at the above periods. An example of the spectrum of the filtered data of 1-day periodicity is shown in Fig. 5b together with the spectrum of original data.

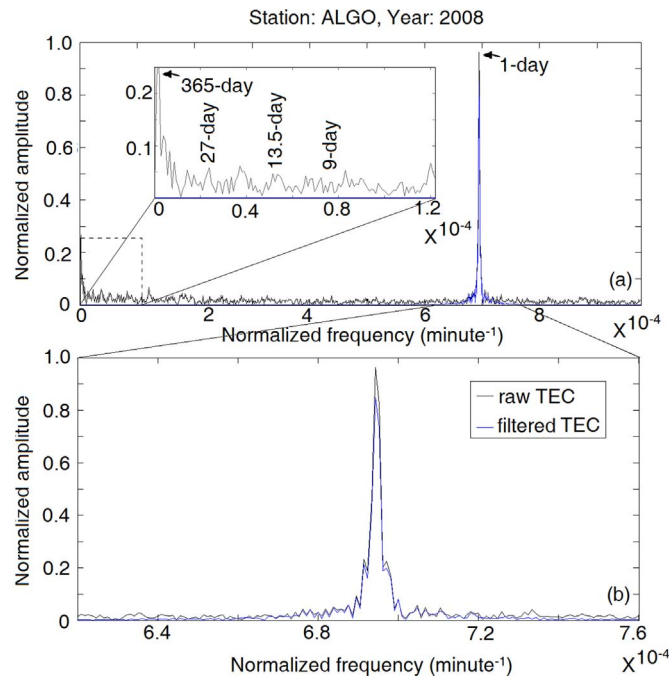


Fig. 5. (a) Fourier spectrum of the raw TEC time series (black line) for the data shown in Fig. 4. Note the well-resolved 1-day periodicity, depicting the fundamental period of TEC. The spectrum of the filtered time series of the one-day period (blue line) is superposed. To highlight the effectiveness of the type-I Chebyshev filter used to isolate the signals of chosen periodicities (see Section 2.2) the enlarged portion of the spectra of raw and filtered data of one-day periodicity are shown in (b). Other well-known periods of solar origin, viz., 27-day, 13.5-day and 9-day have also been shown in the inset in (a). (For interpretation of the references to color in this figure legend, the reader is referred to the web version of this article.)

3. Methodology

To estimate scaling exponents through DFA, the signal under investigation, which can be converted to a self-similar process by integration (Goldberger et al., 2000), should obey the power-law behaviour over various window lengths. Integration would help to unravel the power-law nature by making the signal unbounded and facilitates to detect the underlying self-similarities in the data over various window lengths. The thus generated integrated series is divided into short windows (of equal length) and the average fluctuations associated with each window of data are obtained by calculating the trend (a least-squares fit of chosen order) of the data in each selected window and removing it from each data point of the corresponding window. This is repeated for various window lengths of data. The fractal scaling exponent then signifies the slope of the linear least-squares regression between the logarithm of overall average fluctuations and the logarithm of window lengths (see Subhakar and Chandrasekhar (2015) and references therein) for detailed mathematical description of DFA technique. In MFDFA, the above procedure is carried out repeatedly for different orders of fluctuation functions (also known as moments) in a modified least-squares sense. The entire description of MFDFA technique in simple mathematical steps is described below.

1. First generate an integrated series $y(m)$ of N - point data sequence, say, $x(i)$, by estimating

$$y(m) = \sum_{i=1}^m (x(i) - \bar{x}) \quad ; \quad m = 1, 2, 3, \dots, N \tag{5}$$

\bar{x} designates the mean of the N data points.

2. Next, divide the m -length integrated series into various m/k non-overlapping windows of equal length, each consisting of k number of samples. Thus the total number of windows is, $N_k = \text{int}(m/k)$.
3. Calculate the least-squares fit of preferred order to the data points in each window. This represents the local trend y_k .
4. Detrend the integrated series $y(m)$ by subtracting the local trend y_k from the corresponding window. For a window of length, k , calculate the average fluctuations, $F(k, n)$, of the detrended series in forward and backward directions by

$$F(k, n) = \sqrt{\frac{1}{k} \sum_{i=s+1}^{nk} [y(i) - y_k(i)]^2} \tag{6}$$

where, $s = (n - 1)k$; n depicts the window number. $n = 1, 2, 3, \dots, N_k$ for forward operation and $n = N_k, N_k - 1, N_k - 2, \dots, 2, 1$ for backward operation.

5. Considering both forward and backward operations, the generalised form for overall average fluctuations is expressed as q^{th} order fluctuation function as (Kantelhardt et al., 2002)

$$F_q(k) = \left\{ \frac{1}{2N_k} \sum_{n=1}^{2N_k} [F^2(k, n)]^{q/2} \right\}^{1/q} \tag{7}$$

Eq. (7) is iteratively calculated for various window lengths, k^1 and q values, to provide a power-law relation between $F_q(k)$ and $k^{h(q)}$. The generalised Hurst exponent $h(q)$ defines the slope of the linear least-squares regression between the logarithm of the overall average fluctuations $F_q(k)$ and the logarithm of the window length k , for corresponding q . Generally, Eq. (7) is calculated for various q ranging from -8 to 8 . However, for better characterization of the signal, further higher or lower bounds of q can be chosen. For the case of $q = 0$ (as the exponent becomes divergent at this value), Eq. (7) will be transformed to a logarithmic averaging procedure, given by (Kantelhardt et al., 2002)

¹ According to Peng et al. (1994), the successive window lengths, k , are increased by a factor of $\sqrt[3]{2}$.

$$F_0(k) = \exp\left[\frac{1}{4N_k} \sum_{n=1}^{2N_k} \ln\{F^2(k, n)\}\right] \approx k^{h(0)} \quad (8)$$

The behaviour of multifractal Hurst exponent, $h(q)$ depends on the average fluctuations $F_q(k)$. It bears a non-linear relation with the order of the fluctuation function, q , such that the low (high) average fluctuations have high (low) $h(q)$ for negative (positive) q (Kantelhardt, 2002). If $h(q)$ varies (remains constant) for various q , then the signal is said to have multifractal (monofractal) behaviour. This can be checked by $q, h(q)$ plot.

6. Next, estimate the multifractal singularity spectrum, defining the relation between the singularity spectrum, $f(\alpha)$ and strength of the singularity, α , defined by $f(\alpha) = q[\alpha - h(q)] + 1$ and $\alpha = h(q) + qh'(q)$. α is also known as Hölder exponent. The reader is referred to Kantelhardt et al. (2002) for more details on α and $f(\alpha)$. The shape of singularity spectrum resembles that of a Gaussian curve. Fig. 6 shows an example plot of multifractal singularity spectrum depicting different parameters required to interpret the spectrum. The broader (narrower) the singularity spectrum, the stronger (weaker) the multifractal nature of the signal (Kantelhardt et al., 2002).

3.1. Application of MF DFA to TEC data

TEC data sampled at one-minute interval, which is interpolated and then filtered for well-known periods (explained above in Section. 2.2), is subjected to MF DFA. This is done by choosing a minimum window size of 1024 and maximum window size $N/4$ for TEC data with periodicity of 27-day and its harmonics. For 1-day periodicity the minimum window size is chosen as 25,000. The different minimum window sizes for signals of different periods were chosen by trial-and-error method, so as to ensure that changes in the $F_q(k)$ values (see Eq. (7)) with respect to increase in window sizes corresponding to each q are rather gradual than abrupt. This provides a well-estimated Hurst exponent. As mentioned by Peng et al. (1994), the successive window lengths are incremented by a factor, $\sqrt[8]{2}$. The generalised Hurst exponents $h(q)$ have been determined by varying q between -8 and 8 . In each window, the detrending of the data was done by estimating the linear least-squares fit of the data and then the average fluctuations were determined.

Table 2 depicts the geomagnetic latitude-wise classification of all the stations considered in the present study. The estimated multifractal spectral widths of all stations in each latitude zone corresponding to each period are averaged, and a representative station, whose spectral width is close to this average value is considered to describe the multifractal behaviour of TEC of that particular period of that latitude zone. Fig. 7 shows the multifractal singularity spectra (Fig. 7a-c) and Hurst exponent plots (Fig. 7d-f) determined for the periods of 27-day and its harmonics and 1-day corresponding to the solar minimum year, 2008 (red) and solar maximum year, 2014 (blue) of a representative station in equatorial region (Figs. 7a, d), mid latitude region (Figs. 7b, e) and high latitude region (Figs. 7c, f). Table 3 shows the average multifractal spectral widths determined for each latitude zone corresponding to each period of the years 2008 and 2014.

4. Results and discussion

The multifractal singularity spectra and the generalised Hurst exponents (Fig. 7) are the diagnostic information used to study the multifractal behaviour of TEC. The Hurst exponent, $h(q)$, in general, bears a non-linear relationship with the moments q . However, based on the nature of data under investigation, $h(q)$ may vary (remain constant) with q , in which case, the signal is considered to be multifractal (monofractal) in nature. Secondly, the width of the multifractal singularity spectra ($\alpha_{\max} - \alpha_{\min}$; see Fig. 6) determines the degree of multifractality of a signal and thus the broader (narrower) the

singularity spectrum, the stronger (weaker) the multifractal nature of the signal (Kantelhardt et al., 2002; Subhakar and Chandrasekhar, 2016). The $h(q)$ values estimated for equatorial (Fig. 7d), mid latitude (Fig. 7e) and high latitude (7f) zones of all periods clearly show a distinct behaviour for 27-day period and its harmonics and 1-day period. In case of former, the $h(q)$ values at all latitude zones are greater than 1.0 and for the latter, they are less than 1.0 (Fig. 7d-f). This clearly supports our observation that the 27-day period and its harmonics display the presence of persistent slow-evolving fluctuations, while the 1-day period possesses persistent fast-evolving fluctuations (Kantelhardt et al., 2002; Telesca et al., 2004). The $h(q)$ values of less than 0.5 for 1-day period further suggest that they display antipersistent correlations, indicating successive correlations are somewhat random with increase in window lengths (cf. Eq. 6). On the other hand, the $h(q)$ values of greater than 0.5 for 27-day period and its harmonics display persistent long-term correlations, indicating successive correlations progressively increase with increasing window lengths.

The $f(\alpha)$ vs. α plot, depicting the multifractal singularity spectra (Fig. 6) provide a clear information about the relative presence of small and large fluctuations in the signal under investigation. If a large portion of the spectrum is tilted to the right (that means, in Fig. 6 if $b > a$), with respect to the maximum spectral value ($f_{\max}(\alpha)$), then the spectra accordingly is defined as right skewed. Otherwise (that is, if $b < a$) the spectrum is defined as left skewed. The right (left) skewed spectrum signifies the presence of finer (coarser) structures in the data. Such observations have direct relevance to the shape of Hurst exponent ($h(q)$) plots, drawn as a function of q (Fig. 7d-f), such that, the Hurst exponents corresponding to negative (positive) q correspond to the right (left) portion of the spectra with respect to $f_{\max}(\alpha)$. This can also be easily verified with Eq. (7).

As can be clearly seen in Fig. 7a-c, the multifractal singularity spectra corresponding to the periods of 27-day and its harmonics at all latitude zones uniquely show that the spectra are largely right-skewed. This indicates that the chosen optimal minimum window size of 1024 points corresponding to these periods clearly demonstrates that the data by-and-large possess finer structures (smaller fluctuations). Interestingly, such right-skewed spectral behaviour has been consistent in the data even at high latitude regions for these periods (Fig. 7c). Among all the latitude zones, the multifractal spectral widths corresponding to all periods of 2008 and 2014 of equatorial zone is smaller compared to those of mid and high latitude zones (Table 3). Perhaps this could be attributed either to the seasonal variations in the length of the daytime period which increases with geographic latitude or due to the TEC variability or both. At equatorial region, although the day-to-day TEC variability is highly dynamic, the average seasonal variation is consistent. However, at mid latitudes, while the seasonal diurnal time

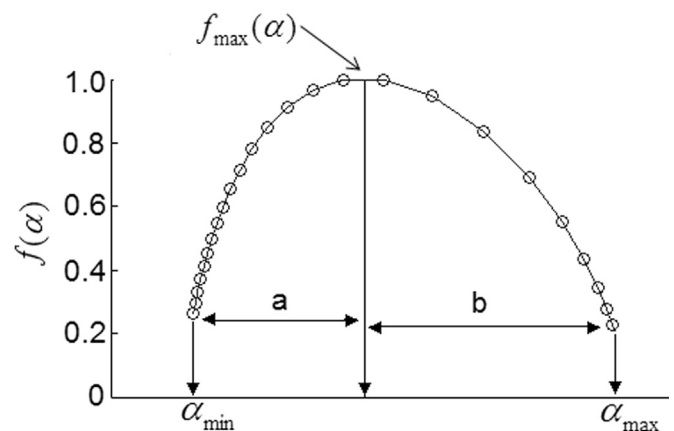


Fig. 6. A cartoon of a typical multifractal singularity spectrum, depicting various parameters that aid in clear understanding of the spectrum.

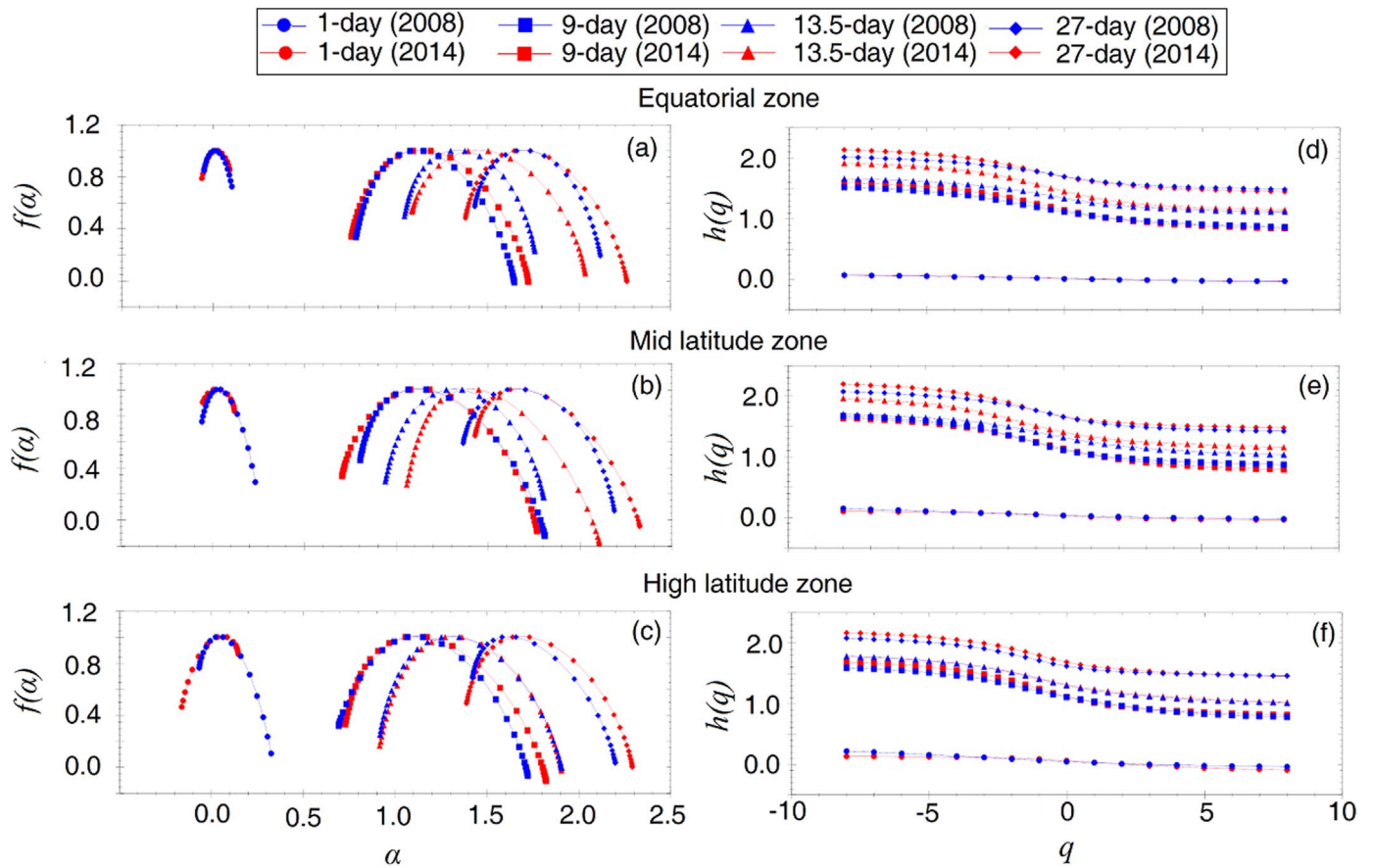


Fig. 7. Comparison of multifractal singularity spectra (a–c) and generalised Hurst exponent plots (d–f) for each of the latitude zones. The solid (red) symbols show data for the solar minimum (maximum) 2008 (2014) corresponding to the periods of 27-day (diamonds), 13.5-day (triangles), 9-day (squares) and 1-day (circle). (For interpretation of the references to color in this figure legend, the reader is referred to the web version of this article.)

Table 3

Comparison of multifractal spectral widths for representative stations of equatorial, mid and high latitude zones for solar minimum year (2008) and solar maximum year (2014) corresponding to the well-known periods of 27-day and its harmonics and 1-day.

Period (in days)	Equatorial Zone		Mid latitude Zone		High latitude Zone	
	2008	2014	2008	2014	2008	2014
1	0.14	0.14	0.28	0.17	0.38	0.30
9	0.87	0.97	1.00	1.06	1.03	1.09
13.5	0.71	0.95	0.86	1.05	0.99	0.99
27	0.69	0.88	0.82	0.89	0.78	0.90

changes dominate the day-to-day TEC variability, at the high latitude regions, the latter is highly dynamic as most of the magnetospheric energy is transmitted into the ionosphere through particle precipitation and ionospheric plasma convection. Such a complex ionospheric scenario often causes large dynamical and chemical disturbances in the high latitude ionosphere, making the TEC highly stochastic in nature. Therefore in accordance with such a complex ionospheric behaviour at different latitudes, the resulting multifractal spectral widths are the largest at high latitude zones, smallest at equatorial zone and intermediary at mid latitude zones.

A careful observation of the multifractal spectra of all periods in Fig. 7a–c suggests that there has been a systematic shift in the spectra towards higher values of α with increase in periods. To ascertain if such a multifractal behaviour of spectra is related to any characteristic feature of ionospheric TEC associated with these periods, we have generated a synthetic data consisting of 27-day period and its harmonics and one-day period of equal number of data points as that

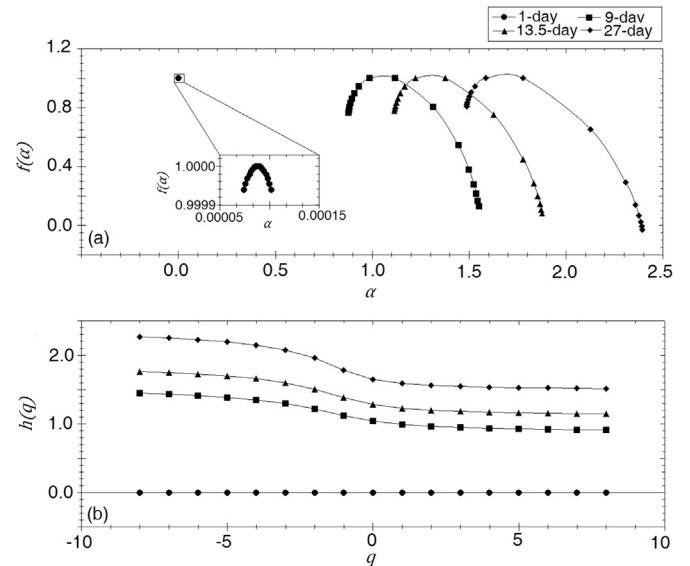


Fig. 8. Comparison of multifractal singularity spectra and Hurst exponents estimated using synthetic data having periods of 27-day variation and its harmonics, and 1-day. The symbols for the above periods are same as those used in Fig. 7 (see Section 4 for more details).

of TEC. Fig. 8 depicts the multifractal singularity spectra obtained for the synthetic data, using the same parameters as used for computing the spectra for TEC data. Interestingly, Fig. 8 also shows a clear spectral shift of larger periods towards higher values of α . This confirms

that the observed shift in the multifractal singularity spectra of TEC towards higher (lower) values of Hölder exponent for larger (smaller) periods during the years of solar minimum and maximum appears to be a natural phenomenon and has no relevance to the degree of solar activity, vis-à-vis the TEC. An interesting observation that can be brought out from Fig. 8 is, that the positioning of multifractal singularity spectrum in the $f(\alpha)$ vs. α plot corresponding to any periodicity in the given data set is dictated by the presence of number of cycles of that periodicity present in the data and thus more number of cycles of any periodicity present in it will have its multifractal spectrum positioned at lower values of α and vice-versa.

Fig. 7a-c also show that except for 1-day period, the multifractal spectral widths increase with decrease in period regardless of solar activity, implying that the degree of multifractality increases with decrease in period. The 27-day period (which is associated with solar rotation) will have similar influence on the TEC multifractal spectra at all latitudes irrespective of the seasonal effect at the latitudes which is more deterministic (further deterministic during low solar period). However, as the period decreases from 27-day to its second (13.5-day) and third (9-day) harmonics, other TEC dynamic variations contribute and the spectral width increases. For example, while the 13.5-day variation may to some extent largely be influenced by semi-lunar tidal effects, the 9-day period may be influenced by day-to-day TEC variability. This has been the case at all latitude zones (see Table 3).

As can be seen from Fig. 7 (see also Table 3), except for 1-day period, the average degree of multifractality is high for periods of 27-day and its harmonics during the solar maximum year 2014 compared to that in the solar minimum year 2008. This could be due to the solar radiation being more dynamic during solar maximum and the 27-day period and its harmonics will become more stochastic. Therefore during the disturbed 2014, the TEC behaviour corresponding to these periods is expected to be stochastic compared to the quieter 2008. A careful observation of the multifractal spectra of 13.5-day periodicity corresponding to 2008 (blue triangles) and 2014 (red triangles) at all latitude zones (see Fig. 7a-c) reveals an interesting observation. Corresponding to this period, the differences in the widths of the multifractal spectra of 2014 and 2008 gradually decrease from equatorial zone to mid latitude zone and it becomes completely negligible at high latitude zone (see Table 3). This could be mainly due to the semi lunar tidal influence on TEC, which is large at equatorial zone and weak at high latitude zones (Siddiqui et al., 2015), indicating that multifractal behaviour at high latitude zones is completely devoid of any lunar influence and thus is solely attributed to solar origin. As well known, the semi lunar tidal effect has a dominant periodicity of 14.5 days, which is close to the 13.5-day periodicity.

A closer look at the multifractal spectra corresponding to 1-day period reveals interesting observations (Fig. 7). First, it exhibits monofractal behaviour regardless of the solar activity. This is because, it is the fundamental period in the TEC time series, showing a distinct peak in the FFT spectrum at this period (i.e. at the frequency, $0.000694 \text{ min}^{-1}$) (Fig. 5). Secondly, at equatorial and mid latitude zones, the spectra of 1-day period are right-skewed corresponding to solar minimum and maximum years. However, at high latitude zone while the 2008 data shows a right skewed spectrum, the 2014 spectrum is a left-skewed one. In general, while a right-skewed multifractal spectrum signifies a strongly weighted high fractal exponents, corresponding to finer structures present in the data, the relatively low values of fractal exponents, representative of larger structures account for left-skewed spectra. A closer look at the data of the representative sites of these zones (Fig. 2) reveals that the 2014 data displays a dominant seasonal influence compared to 2008, resulting low amplitudes in the months of May to August at all latitude zones. Particularly at high latitude zone, the seasonal influence and charge precipitation have further reduced amplitudes of the TEC, thereby making them responsible for the left-skewed spectra during the solar active period. Perhaps this could also be attributed to highly heterogeneous nature of

TEC data at high latitude zone compared to equatorial and mid latitude zones. The present study paves a thorough path for extending such studies involving further better understanding of the spatio-temporal variations of TEC using satellite data.

5. Conclusions

MFDFA has been shown to be one of the efficient nonlinear mathematical techniques to analyze nonlinear and nonstationary data, such as TEC, to provide quantitative estimates of stochasticity present in the data. The delineated multifractal behaviour of TEC adds a further dimension to the existing understanding about the latitudinal dependence of TEC, vis-à-vis the solar activity. Through multifractal singularity spectra of 13.5-day period, the semi lunar tidal influence on TEC became significantly evident at equatorial zones, while it completely wanes away at high latitude zones. Particularly at high latitude zone, while the seasonal influence and the charge precipitation did not largely influence the longer period data, they did effect the 1-day period of TEC resulting in left-skewed multifractal spectra during the solar active period. The observed shift in the multifractal singularity spectra of TEC towards lower (higher) values of Hölder exponent for smaller (larger) periods during the years of solar minimum and maximum appears to be a natural phenomenon and has no relevance to the degree of solar activity. All the above interesting observations concerning the characterization of TEC at different latitude zones during solar minimum and maximum periods was possible because of the effective prediction of the missing data with least error by implementing a special linear interpolation technique and by using type-I Chebyshev bandpass filter for precise selection of narrow band of frequencies centered at different periods considered in the present study. We strongly believe that by using TEC data of more than a year or two, the seasonal variability in TEC vis-à-vis solar activity can be effectively studied using MFDFA. Also, this work forms an excellent guide for extending multifractal studies to characterize satellite TEC data.

Acknowledgements

The authors thank SOPAC facility for maintaining and making available the high quality TEC data, without which the present analysis could not have been possible. One of the authors, EC thanks Prof. Hermann Lühr for stimulating discussions on the interpretation of TEC data, particularly corresponding to the 13.5-day period of TEC. SP thanks the Department of Earth Sciences, IIT Bombay for extending all the required facilities and Goa University, for permitting her to carry out this work at IIT Bombay. The authors also thank the editor, Prof. Dora Pancheva and two anonymous referees for their positive words of encouragement and comments, which have improved the original version of the paper.

References

- Bhuyan, P.K., Borah, R.R., 2007. TEC derived from GPS network in India and comparison with IRI. *Adv. Space Res.* 39, 830–840. <http://dx.doi.org/10.1016/j.asr.2006.12.042>.
- Borries, C., Jakowski, N., Jacobi, Ch, Hoffmann, P., Pogoreltsev, A., 2007. Spectral analysis of planetary waves seen in ionospheric total electron content (TEC): first results using GPS differential TEC and stratospheric reanalyses. *J. Atmos. Sol. Terr. Phys.* 69, 2442–2451. <http://dx.doi.org/10.1016/j.jastp.2007.02.004>.
- Dasgupta, A., Paul, A., Das, A., 2007. Ionospheric total electron content (TEC) studies with GPS in the equatorial region. *Ind. J. Radio Space Phys.* 36, 278–292.
- Ercha, A., Zhang, D., Ridley, A.J., Xiao, Z., Hao, Y., 2012. A global model: empirical orthogonal function analysis of total electron content 1999–2009 data. *J. Geophys. Res.: Space Phys.* 117 (A03328), 1978–2012. <http://dx.doi.org/10.1029/2011JA017238>.
- Fagundes, P.R., Pillat, V.G., Bolzan, M.J.A., Sahai, Y., Becker-Guedes, F., Abalde, J.R., Aranha, S.L., 2005. Observations of F layer electron density profiles modulated by planetary wave type oscillations in the equatorial ionospheric anomaly region. *J. Geophys. Res.* 110 (A12), A12302. <http://dx.doi.org/10.1029/2005JA011115>.
- Fedrizzi, M., de Paula, E.R., Kantor, L.J., Langley, R.B., Santos, M.C., Komjathy, A., 2002. Mapping the low latitude ionosphere with GPS. *GPS World* 13 (2), 41–46.

- Fernandez, L.I., Meza, A.M., Van Zele, M.A., 2012. Wavelet analysis of the ionospheric response at mid-latitudes during the April 2000 storm using magnetograms and VTEC from GPS. *Geoacta* 37 (2), 178–196.
- Goldberger, A.L., Amaral, L.A.N., Glass, L., Hausdorff, J.M., Ivanov, P.Ch, Mark, R.G., Mietus, J.E., Moody, G.B., Peng, C.-K., Stanley, H.E., 2000. Physiobank, physiotookit, and physionet, components of a new research resource for complex physiologic signals. *Circulation* 100 (10), e215–e220. <http://dx.doi.org/10.1161/01.CIR.101.23.e215>.
- Grinsted, A., Moore, J.C., Jevrejeva, S., 2004. Application of the cross wavelet transform and wavelet coherence to geophysical time series. *Nonlinear Process. Geophys.* 11, 561–566. SRef-ID: 1607-7946/npg/2004-11-561.
- Gulyaeva, T.L., 1999. Regional analytical model of ionospheric total electron content: monthly mean and standard deviation. *Radio Sci.* 34, 1507–1512.
- Huang, C.S., 2008. Global characteristics of ionospheric electric fields and disturbances during the first hours of magnetic storms. *Adv. Space Res.* 41, 527–538.
- Kantelhardt, J.W., Zschiegner, S.A., Koscielny-Bunde, E., Havlin, S., Bunde, A., Stanley, H.E., 2002. Multifractal detrended fluctuation analysis of nonstationary time series. *Physica A* 316, 87–114. [http://dx.doi.org/10.1016/S0378-4371\(02\)01383-3](http://dx.doi.org/10.1016/S0378-4371(02)01383-3).
- Klobuchar, J. A., 1991. Ionospheric effects on GPS, Innovation, Reprinted from GPS World.
- Klobuchar, J.A., 1996. Ionospheric effects on GPS. In: Spilker, J.J., Parkinson, B.W. (Eds.), *Global positioning system: theory and applications* 1. AIAA, 485–515.
- Krankowski, A., Kosek, W., Baran, L.W., Popinski, W., 2005. Wavelet analysis and forecasting of VTEC obtained with GPS observations over European latitudes. *J. Atmos. Sol. Terr. Phys.* 67 (12), 1147–1156. <http://dx.doi.org/10.1016/j.jastp.2005.03.004>.
- Lin, J., 2010. Two-dimensional ionospheric total electron content map (TEC) seismo-ionospheric anomalies through image processing using principal component analysis. *Adv. Space Res.* 45 (11), 1301–1310. <http://dx.doi.org/10.1016/j.asr.2010.01.029>.
- Lin, J., 2011a. Latitude-time total electron content anomalies as precursors to Japan's large earthquakes associated with principal component analysis. *Int. J. Geophys.*, 763527. <http://dx.doi.org/10.1155/2011/763527>.
- Lin, J., 2011b. Principal component analysis method in the detection of total electron content anomalies in the 24 h prior to large earthquakes. *Arab. J. Geosci.* 4, 575–593. <http://dx.doi.org/10.1007/s12517-010-0204-4>.
- Liu, L., Chen, Y., 2009. Statistical analysis of solar activity variations of total electron content derived at Jet Propulsion Laboratory from GPS observations. *J. Geophys. Res.* 114, A10311. <http://dx.doi.org/10.1029/2009JA014533>.
- Mannucci, A.J., Wilson, B.D., and Edwards, C.D., 1993. A new method for monitoring the earth's ionospheric total electron content using the GPS global network, In: *Proceedings of the 6th International Technical Meeting of the Satellite Division of The Institute of Navigation (ION GPS 1993)*, Salt Lake City, UT, pp. 1323–1332.
- Meza, A., Van Zele, M.A., Brunini, C., Cabassi, I.R., 2005. Vertical electron content and geomagnetic perturbations at mid- and sub-auroral southern latitudes during geomagnetic storms. *J. Atmos. Sol. Terr. Phys.* 67, 315–323. <http://dx.doi.org/10.1016/j.jastp.2004.07.042>.
- Otsuka, Y., Ogawa, T., Saito, A., Tsugawa, T., Fukao, S., Miyazaki, S., 2002. A new technique for mapping of total electron content using GPS network in Japan. *Earth Planets Space* 54, 63–70.
- Pancheva, D., 2006. Planetary wave coupling of the low latitude atmosphere-ionosphere system. In: *Proceedings of the 36th COSPAR Scientific Assembly*, 36, 2045.
- Pancheva, D., Mukhtarov, P., 2000. Wavelet analysis on transient behaviour of tidal amplitude fluctuations observed by meteor radar in the lower thermosphere above Bulgaria. *Ann. Geophys.* 18, 316–331.
- Peng, C.-K., Buldyrev, S.V., Havlin, S., Simons, M., Stanley, H.E., Goldberger, A.L., 1994. Mosaic organization of DNA nucleotides. *Phys. Rev. E* 49 (2), 1685–1689.
- Pervak, S., Choliy, V., Taradiy, V., 2008. Spectral analysis of the ionospheric irregularities from GPS observations. In: *Proceedings of the WDS'08, Part-II*, pp. 189–191, (isbn:978-80-7378-066-1)
- Proakis, J.G., Monolakis, D.G., 1996. Design of digital filters (Chapter 08), *Digital Signal Processing, Principles, Algorithms and Applications*, Third edition, pp. 682–689.
- Pröls, G.W., 1993. On explaining the local time variation of ionospheric storm effects. *Ann. Geophys.* 11, 1–9.
- Rama Rao, P.V.S., Seemala, G.K., Niranjan, K., Prasad, D.S.V.V.D., 2006. Temporal and spatial variations in TEC using simultaneous measurements from the Indian GPS network of receivers during the low solar activity period of 2004–2005. *Ann. Geophys.* 24 (12), 3279–3292, < hal-00318232 > .
- Seemala, G.K., Valladares, C.E., 2011. Statistics of total electron content depletions observed over the South American continent for the year 2008. *Radio Sci.* 46 (RS5019), 2011. <http://dx.doi.org/10.1029/2011RS004722>.
- Shagimuratov, I.I., Chernyak, Y.V., Zakharenkova, I.E., Yakimova, G.A., 2013. Use of total electron content maps for analysis of spatial–temporal structures of the ionosphere. *Russ. J. Phys. Chem. B* 7 (5), 656–662.
- Siddiqui, T.A., Stolle, C., Lühr, H., Matzka, J., 2015. On the relationship between weakening of the northern polar vortex and the lunar tidal amplification in the equatorial electrojet. *J. Geophys. Res. Space Phys.* 120 (11), 10,006–10,019. <http://dx.doi.org/10.1002/2015JA021683>.
- Subhakar, D., Chandrasekhar, E., 2015. Detrended fluctuation analysis of geophysical well-log data. In: Dimri, V.P. (Ed.), *Fractal Solutions for Understanding Complex Systems in Earth Sciences* 2nd edition. Springer International Publishing, Switzerland, 47–65. http://dx.doi.org/10.1007/978-3-319-24675-8_4.
- Subhakar, D., Chandrasekhar, E., 2016. Reservoir characterization using multifractal fluctuation analysis of geophysical well-log data. *Physica A* 445, 57–65. <http://dx.doi.org/10.1016/j.physa.2015.10.103>.
- Telesca, L., Lapenna, V., Macchiato, M., 2004. Mono- and multi-fractal investigation of scaling properties in temporal patterns of seismic sequences. *Chaos Solitons Fractals* 19, 1–15. [http://dx.doi.org/10.1016/S0960-0779\(03\)00188-7](http://dx.doi.org/10.1016/S0960-0779(03)00188-7).
- Wang, X., Sun, Q., Eastes, R., Reinisch, B., Valladares, C.E., 2008. Short-term relationship of total electron content with geomagnetic activity in equatorial regions. *J. Geophys. Res.* 113, A11308. <http://dx.doi.org/10.1029/2007JA012960>.
- Wessel, P., Smith, W.H.F., Scharroo, R., Luis, J.F., Wobbe, F., 2013. *Generic Mapping Tools: improved version released*. EOS Trans. AGU 94, 409–410.
- Zheng, J., Zhao, B., Xiong, B., Wan, W., 2016. Spatial and temporal analysis of the total electron content over China during 2011–2014. *Adv. Space Res.* <http://dx.doi.org/10.1016/j.asr.2016.03.037>.